Transient Analysis of Short, High-Concentration, Gain-Clamped Er^{3+}-Yb^{3+} Codoped Fiber Amplifiers

Eldad Yahel, Ortwin Hess, and Amos A. Hardy, *Fellow, IEEE*, *Fellow, OSA*

***Abstract*—A theoretical study of the dynamics of short high–concentration gain-clamped Er^{3+}-Yb^{3+} codoped fiber amplifiers is presented. The effect of various parameters on the transient power excursions and relaxation oscillation frequency of a given signal input channel when other signal channels are added or dropped from an initial steady-state configuration is analyzed. In particular, the effects of Er^{3+} clustering, Yb^{3+} concentration, fiber length, lasing wavelength, pump wavelength, pump power, and cavity losses are shown. The numerical results demonstrate the importance of Yb^{3+} sensitization in achieving stable gain–clamped operation in a range of operating conditions. It is shown that the amplitude of power excursions is typically small, e.g., less than 0.1 dB, provided that the amount of Er^{3+} ions in the clusters is kept small.**

***Index Terms*—Erbium (Er), gain clamping, optical fiber amplifiers, wavelength-division multiplexing (WDM), ytterbium (Yb).**

I. Introduction

SHORT Er^{3+}-doped fiber amplifiers (EDFAs) are attractive, low-cost, and compact devices for optical communication applications in the wavelength range of 1.55 μm. To increase the gain per unit length along the typically centimeters-long fiber, high Er^{3+} concentrations are required. This requirement limits the achievable gain due to the presence of Er^{3+} ion–ion interactions [1]. It is thus preferable to employ glasses that have a small homogeneous upconversion coefficient, e.g., phosphate glass, as the host material for short EDFA [2], [3]. Another important requirement for short fiber amplifiers is to maximize the pump absorption along the fiber and hence improve the amplifier conversion efficiency. To this end, Er^{3+}-Yb^{3+} codoped fiber amplifiers (EYDFAs) allow to increase the pump efficiency of Er^{3+} ions, as Yb^{3+} codoping provides an indirect energy-transfer mechanism from the Yb^{3+} to the Er^{3+} ions. Also, Yb^{3+} has a very broad absorption spectrum extending from approximately 850 to 1000 nm (compared with the more narrow absorption bands of Er^{3+}, e.g., at 976 nm). These properties have led to the recent realization of efficient and short EYDFAs [4].

An important design issue for fiber amplifiers that operate in the multiwavelength regime, i.e., for wavelength-division-multiplexing (WDM) applications, is the limitations of the power transients of the amplified signals when saturation conditions change [5]. This consideration is of particular importance in access/metro WDM networks where input signal channels are being added or dropped due to reconfiguration. One method to achieve automatic stabilization is to introduce a lasing channel outside the signal bandwidth to clamp the length-averaged amplifier population inversion and, hence, the gain [6], [7]. In considering the gain-clamping mechanism, one should take into account that the fraction of clustered Er^{3+} ions can be quite significant in high-concentration fibers [8], [9]. This can render gain clamping to be ineffective due to laser self-pulsation induced by the Er^{3+} clusters [10]–[12]. Yb^{3+} codoping can stabilize the lasing channel, as it increases the pump efficiency and counteracts the negative effect of Er^{3+} ion–ion interactions [12]. In addition, the improved pump absorption in short EYDFAs allows to realize cladding-pumped fiber geometry with higher output powers [13]. This can be useful for power boosting applications [14].

Previous theoretical works have studied the dynamic behavior of low-concentration gain-clamped EDFAs, e.g., [15]–[18]. The dynamics of gain-clamped EYDFAs was recently considered in [19], [20] both experimentally and with an approximate model. In particular, it was demonstrated that increasing the effective pump power or decreasing the fiber length can limit the surviving channel power transients of relatively long (i.e., meters) gain-clamped EYDFAs. Our goal in this contribution is to further extend these works and to study the dynamic characteristics of short (i.e., centimeters), high-concentration, gain-clamped EYDFAs, operating in the gain-flattened regime. We propose this configuration as a compact, cost-effective, automatically gain-stabilized, optical amplifier for WDM metro networks, with transmission latency that is considerably smaller compared with longer amplifiers. We demonstrate the effects of Er^{3+} clustering, and the effect of the Yb^{3+} concentration, on the dynamics of such amplifiers. We also consider the effect of various important amplifier design parameters, such as the fiber length, laser wavelength, pump wavelength, pump power, and cavity losses, on the dynamic performance. For this purpose, we employ a comprehensive coupled propagation-rate equations model, which we have recently introduced [21]. Our model takes into account the energy transfer between the Yb^{3+} and Er^{3+} ions, the presence of Er^{3+} clusters, as well as amplified spontaneous emission (ASE) in the vicinity of the signal and pump wavelengths. The model assumes homogeneous broadening mechanisms, and therefore, it does not account for the static contribution of the spectral hole burning to the dynamic power excursion [15].

Manuscript received September 8, 2005; revised February 1, 2006. The work of A. A. Hardy was supported by the Chana and Heinrich Manderman Chair in Optoelectronics at Tel-Aviv University.

E. Yahel and O. Hess are with the Advanced Technology Institute, University of Surrey, Surrey, Guildford GU2 7XH, U.K. (e-mail: E.Yahel@surrey.ac.uk; O.Hess@surrey.ac.uk).

A. A. Hardy is with the Laboratory of Physics of Nanostructures, Ecole Polytechnique Fédérale de Lausanne, Lausanne 1015, Switzerland, and also with the Department of Electrical Engineering–Physical Electronics, Tel-Aviv University, Tel-Aviv 69978, Israel (e-mail: hardy@eng.tau.ac.il).

Digital Object Identifier 10.1109/JLT.2006.872264

This paper is organized as follows. In Section II, we briefly give the main assumptions leading to the theoretical model for the Er^{3+}-Yb^{3+} codoped fiber, which was given in detail in [21]. In particular, we discuss the choice of model parameters. In Section III, we consider some numerical examples for cladding-pumped, gain-clamped EYDFAs that operate in the conventional band (C-band) of the Er^{3+} gain spectrum. Conclusions are drawn in Section IV. In the Appendix, we introduce a recursive finite-difference solution scheme for the dynamic spectral power densities propagation equations, which takes in account the exact boundary conditions at the fiber ends.

II. Theoretical Model

We assume a step-index fiber geometry of length L, with distributed Bragg reflector (DBR) mirrors on either side that provide optical feedback in selective wavelengths for automatic gain clamping [7]. The light that is amplified and generated in the cavity, with spectral power densities $P^{\pm}_{\rm Er}(z,t,\lambda)$ and $P^{\pm}_{\rm Yb}(z,t,\lambda)$, due to transitions by either the Er^{3+} or Yb^{3+}, respectively, propagate in both the forward (positive) and backward (negative) z-direction. It is assumed that the fiber is single mode at any wavelength in the vicinity of a signal wavelength λ_s. The power that propagates in the radiation modes is neglected because it is much weaker than the power guided in the fundamental mode. Therefore, the coupling of the light field with the fiber core can be described by the power filling factor $\Gamma(\lambda)$ of the fundamental LP_{01} mode. An approximate expression for this parameter is derived in [22]. The pump power $P^{+}_{p}(z,t)$ at wavelength $\lambda=\lambda_p$ is injected into the fiber at $z=0$ and propagates along the forward z-direction. For single-clad fibers, we assume that the pump power filling factor Γ_p satisfies $\Gamma_p \simeq \Gamma(\lambda_p)$. For double-clad fibers, we assume that the first cladding geometry favors rapid pump modes mixing along the fiber length (e.g., by placing the core offset the center of cladding) [23]. In this case, we might assume that pump absorption is essentially uniform with an effective pump power filling factor that is approximately given by $\Gamma_p \simeq A_{\rm core}/A_{\rm clad}$. Here, $A_{\rm core}$ is the fiber core area, and $A_{\rm clad}$ is the first cladding area (including the core).

The fiber core is uniformly doped with Er^{3+} and Yb^{3+} with concentrations N_{Er} and $N_{\rm Yb}$, respectively. Our model takes into account pump absorption by Er^{3+} and Yb^{3+} ions, forward and backward energy transfer, ASE, and scattering losses [21]. The model assumes physical clustering of Er^{3+} ions. That is, the fiber core contains two types of ion populations, namely, homogeneously mixed Er^{3+} and Yb^{3+} ions and a clustered population of Er^{3+} ions that are not coupled to the Yb^{3+} ions and therefore are not excited by the Yb^{3+} energy transfer [21]. The fraction of Er^{3+} ions in clusters is given by k. We model homogeneous and intracluster upconversion of Er^{3+} ions using a quadratic term in the rate equations [24], with rate coefficients C_2 and $\bar{C}_2$, respectively (cf. Table I). We note that C_2 depends strongly on the host glass properties [25], and we assume that it increases linearly with the Er^{3+} concentration [2]. The cross-relaxation coefficients R_{61} and R_{35} for the forward and backward Yb^{3+}-Er^{3+} energy-transfer process, respectively, are assumed to be of the same magnitude [26] and to depend linearly on the Yb^{3+} concentration [2]. We note that the existence of Yb^{3+} clusters and cumulative energy-transfer losses to the Er^{3+} $^2I_{13/2}$ state can be significant in silica-based EYDFAs [27]. However, further experimental data are required to elucidate the relative strength of this loss mechanism in high-concentration phosphate-based EYDFAs. To be on the safe side, we restrict the calculations to relatively low Yb^{3+}-Er^{3+} ratios, e.g., $N_{\rm Yb}/N_{\rm Er} \le 5$, so that every Yb^{3+} ion can be assumed to be coupled to the nearby Er^{3+} ions only [28].

TABLE I
Parameters Used in the Numerical Calculations

Parameter	Value	Notes
λ_p	976 nm	
τ_{21}	7.9 msec	Ref. [32]
τ_{32}	2 μsec	Ref. [33]
τ_{65}	2.2 msec	Ref. [2]
$\sigma_{13}(\lambda)$		Ref. [2]
$\sigma_{12}(\lambda)$, $\sigma_{21}(\lambda)$		Ref. [32]
$\sigma_{56}(\lambda)$, $\sigma_{65}(\lambda)$		Ref. [34]
C_2	1.3×10^{-24} m^{3}sec^{-1}	Based on Ref. [2]
$\bar{C}_2$	1×10^{-20} m^{3}sec^{-1}	Based on Ref. [35]
R_{61}, R_{35}		Based on Ref. [2]
α	6.45 m^{-1}	Ref. [4]
n	1.55	Ref. [32]
$\Gamma(\lambda)$		Ref. [22]
A_{core}	3.42×10^{-11} m^2	
NA	0.16	
Γ_p	0.01	
N_{Er}	5×10^{26} m^{-3}	
N_{Yb}	1.5×10^{27} m^{-3}	
k	0	

The model includes signal and pump scattering losses α and single-ion transitions between levels i and j that are characterized by wavelength-dependent emission and absorption cross sections $\sigma_{ij}(\lambda)$, as well as finite transitions lifetimes τ_{ij} [21]. We consider the ASE power induced by the $^2F_{5/2}$–$^2F_{7/2}$ transitions of Yb^{3+} in the range of 900–1060 nm and the ASE power induced by the $^4I_{13/2}$–$^4I_{15/2}$ transitions of Er^{3+} ions in the range of 1417–1649 nm. The propagation equations for the Er^{3+} and Yb^{3+} ASE spectral power densities, and for the pump power, are given by [21, Eqs. (11)–(13)], whereas the set of time-dependent rate equations for the homogeneous and clustered ion populations is given by [21, Eqs. (1)–(8)]. To solve these equations, we divide the ASE spectrum into discrete channels of width $\Delta\lambda=1$ nm, whereas the width of a channel in the signal bandwidth is $\Delta\lambda_s \ll \Delta\lambda$. Thus, the signal power is given by $P^{\pm}_{s}(z,t)=P^{\pm}_{\rm Er}(z,t,\lambda_s)\Delta\lambda_s$. We assume throughout this work that the signal channels are injected into the fiber at $z=0$, i.e., in forward pumping configuration. The following boundary conditions are imposed on the lasing wavelength of the Er^{3+} spectral power densities:

$$P^{+}_{\rm Er}(0,t,\lambda)=R_1(\lambda)P^{-}_{\rm Er}(0,t,\lambda) \tag{1a}$$

$$P^{-}_{\rm Er}(L,t,\lambda)=R_2(\lambda)P^{+}_{\rm Er}(L,t,\lambda). \tag{1b}$$

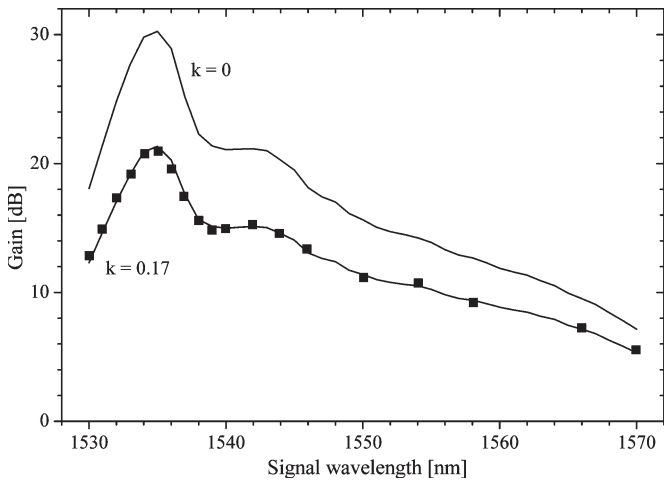

Fig. 1. Gain versus the signal wavelength for two different relative number of Er^{3+} ions in clusters (k). The fiber core area is $A_{\rm core} = 1.96 \times 10^{-11}$ m^2, the numerical aperture NA $= 0.21$, the injected signal power $P_s^+(0) = -30$ dBm, the pump power $P_p^+(0) = 224$ mW, and the Er^{3+} and Yb^{3+} concentrations $N_{\rm Er} = 3.02 \times 10^{26}$ m^{-3} and $N_{\rm Yb} = 1.96 \times 10^{26}$ m^{-3}, respectively [4]. Other parameters are given in Table I. The solid lines represent the numerical solution, whereas the rectangles represent experimental data obtained from [4].

Here, the terms R_1 and R_2 are the power reflectivities at $z = 0$ and $z = L$, respectively. We assume that the DBR mirrors can produce a very narrow reflectivity bandwidth, e.g., ~ 0.1 nm, so that it is sufficient to consider a single wavelength reflectivity at the boundaries [29]. Thus, the reflected power represents an average over the excited axial modes. To obtain steady-state solutions, we employ an iterative procedure: integration along the forward and backward propagation directions until the overall signal and ASE power densities are converged [21]. For the time-dependent cases, we use a finite-difference approximation with two separate grids, i.e., 1) one for the ions and 2) one for the photons, with the ions grid shifted by half-time-step $\Delta t/2$ and half-spatial-step $\Delta z/2$, with respect to the photons grid. The finite-difference approximations are given in the Appendix, where we also describe the integration procedure of the equations with the given boundary conditions (1).

The validity of the model equations has been demonstrated in the case of continuous-wave high-power EYDFAs [30] and Q-switched cladding-pumped Er^{3+}-Yb^{3+} codoped fiber lasers [31], with relatively low Er^{3+} concentrations and negligible clustering. To show the effect of clustering, we depict in Fig. 1 the small-signal gain of a 4.4-cm-long core-pumped, high-concentration EYDFA. A similar configuration was studied experimentally in [4] under continuous-wave conditions. We note the excellent agreement between the experimental results and the numerical calculation for a wide range of signal wavelengths, provided that the fraction of clustered Er^{3+} ions is assumed to be $k = 0.17$. Smaller values of k tend to increase the gain in the entire bandwidth of the signal wavelengths.

III. Examples

In this section, we consider a set of examples for cladding-pumped, gain-clamped, C-band EYDFA near the 976-nm pump transition. Unless otherwise stated, we assume that the parameters for the calculations are given in Table I. These parameters correspond to an efficient phosphate-based Er^{3+}-Yb^{3+} codoped fiber. The input signal band consists of ten equally spaced spectral channels in the range 1544–1562 nm, with width $\Delta\lambda_s = 0.375$ pm. This choice is based on the theoretical gain spectrum of Er^{3+} in phosphate glass, which shows that the gain ripple (cf. Fig. 1) can be minimized by properly selecting the amplifier parameters (e.g., pump power and fiber length) to achieve a particular average population inversion. It is assumed that the input pump power is $P_p^+(0) = 2$ W, whereas the total input power of the signal is $P_s^{\rm total} = 0$ dBm, equally distributed among the signal channels. We assume that the Bragg gratings select the lasing wavelength at 1586 nm. The power reflectivities of the DBR mirrors are $R_1 = 0.98$ and $R_2 = 0.04$ at $z = 0$ and $z = L$, respectively. Note that R_2 should be selected small enough to provide high gain for the signal while maintaining stable gain-clamping conditions.

In what follows, we consider the effect of dropping or adding nine out of the ten signal channels from an initial steady-state regime. We assume that the signal power decreases (or increases) instantaneously, as this constitutes the worst case failures in WDM network amplifiers [16]. To this end, the steady-state solutions are used as the initial conditions for the subsequent time evolution.

The amount of Er^{3+} clustering in high-concentration Er^{3+}-Yb^{3+} codoped fibers is somewhat ambiguous. In principle, it depends on several factors, e.g., the Er^{3+} and Yb^{3+} concentrations, and the fiber processing. In particular, high Er^{3+} concentration and low Yb^{3+}-Er^{3+} ratio favor Er^{3+} clustering [28]. To illustrate the effect of Er^{3+} clustering on the dynamics of gain-clamped EYDFAs, we depict in Fig. 2 the transient response of a surviving channel ($\lambda_s = 1562$ nm) when nine channels are dropped at $t = 0$ from initial steady-state conditions. When the signal channels are dropped, the surviving channel output power exhibits transient power excursions due to the relaxation oscillation in the lasing channel [15]. We note that in the limit of negligible amounts of clustered Er^{3+} ions (e.g., $k \simeq 0$), the power transients damp into a constant steady state after a few hundred microseconds. Thus, the dynamic behavior is similar to low-concentration gain-clamped EDFA [15]–[18], but with typically smaller power excursions. With increased amount of Er^{3+} clustering, the period of the relaxation oscillation increases, and there is no oscillations' damping. In fact, there is a limiting value of k, $k_{\rm cr} \simeq 0.1$, for achieving damped oscillations in the laser and the surviving signal output power. For values of k higher than this value, e.g., $k = 0.14$, the amplitude of the oscillations in the laser power increases with time [10], and self-pulsation in the signal power is generated [see Fig. 2(a)]. We note that the pumping process builds up the inversion of the homogeneous Er^{3+} average population between successive pulses [see Fig. 2(b)], whereas the inversion of the clustered Er^{3+} ions becomes depleted in this time interval. Thus, self-pulsation in the signal power is established for effective pumping rates too weak to counteract the fast upconversion process in the clustered Er^{3+} ions during the laser channel relaxation oscillation. It is worth to mention, however, that although an increased amount of Er^{3+} in clusters wastes

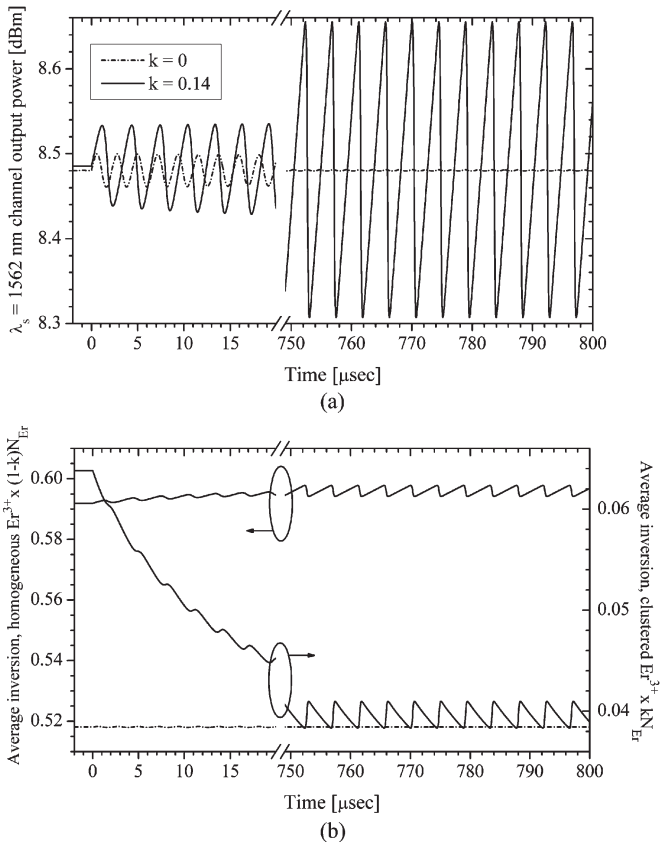

Fig. 2. Transient response of (a) the $\lambda_s = 1562$ nm channel output power and (b) the normalized length-averaged inversion of the homogeneous Er^{3+} population (left side) and the clustered Er^{3+} population (right side). Here, nine out of ten channels are dropped at $t = 0$ from initially steady state, for two different relative number of Er^{3+} ions in clusters (k). The Yb^{3+}-Er^{3+} ratio is $N_{Yb}/N_{Er} = 1$, and the fiber length is $L = 16.5$ cm, for which the gain is approximately flat.

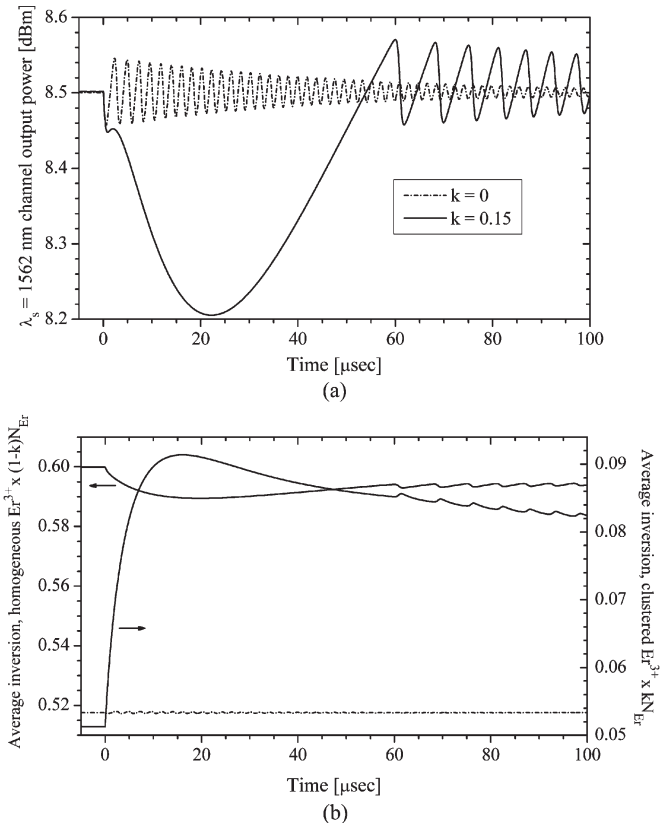

Fig. 3. Same as Fig. 2 when nine channels are added at $t = 0$ from initially steady state. The Yb^{3+}-Er^{3+} ratio is $N_{Yb}/N_{Er} = 3$.

the laser power, and therefore reduces the lasing efficiency, clustering has only a small effect on the amplifier characteristics (e.g., the signal gain, gain flatness, and noise figure) because the overall Er^{3+} population inversion is approximately fixed.

Fig. 3 depicts the transient response of the channel at $\lambda_s = 1562$ nm when channels are added at $t = 0$ to an initial steady-state regime. Here, we also note the similarity between the dynamic behavior of nonclustered gain-clamped EYDFA and the low-concentration gain-clamped EDFA [15]–[18]. The amplification process of the signal saturates the homogeneous Er^{3+} inverted population below the threshold value, and the recovery time of the signal power undershoot depends on the pump efficiency [17]. Increasing the number of clustered Er^{3+} ions also increases absorption losses. This, in turn, increases the undershoot in the signal output power [see Fig. 3(a)]. In fact, we note that for the $k \simeq 0.15$ case, the pumping process rebuilds the average inversion of the homogeneous Er^{3+} ion population toward the laser threshold [see Fig. 3(b)], and the $\lambda_s = 1562$ nm channel power relaxes toward a constant steady-state regime only after several tens of microseconds. We conclude that clustered Er^{3+} ions act as a distributed saturable absorber that inhibits stable gain-clamping conditions if the clustering ratio is too high and the pump power is not strong enough. For example, the delay in the onset of relaxation oscillation (calculated from $t = 0$ until the first oscillations peak) increases from $\Delta t_{oc} \simeq 18.9\ \mu$s to $\Delta t_{oc} \simeq 60\ \mu$s for $k \simeq 0.12$ and $k \simeq 0.15$, respectively.

Next, we consider the effect of the Yb^{3+}-Er^{3+} ratio on the dynamic response of the amplifier. The Yb^{3+} concentration has only a small effect on the Er^{3+} population inversion and hence on the static gain-clamped amplifier characteristics, e.g., the gain flatness. However, the dynamic behavior of high-concentration gain-clamped EYDFAs depends strongly on the value of the Yb^{3+} concentration. Fig. 4 depicts the transient response of the $\lambda_s = 1562$ nm channel output power when channels are (a) dropped and (b) added at $t = 0$ from an initial steady-state regime. Here, different Yb^{3+}-Er^{3+} ratios are assumed for $k = 0.17$ clustering. For a relatively small Yb^{3+}-Er^{3+} ratio (e.g., $N_{Yb}/N_{Er} = 1.5$), the power in the surviving channel following channels' removal shows steady oscillations without damping [cf. Fig. 4(a)]. On increasing the Yb^{3+} concentration, the effective pumping rate also increases, and the oscillation period decreases with time. For the given k, there is a limiting value of Yb^{3+}-Er^{3+} ratio $(N_{Yb}/N_{Er})_{cr} \simeq 2.6$ for which the transient behavior changes from nondamping oscillations into damped oscillations. For sufficiently high Yb^{3+}-Er^{3+} ratio, e.g., $N_{Yb}/N_{Er} = 5$, the relaxation oscillation in the laser channel are strongly damped, resulting in constant output power of the surviving signal within few hundred microseconds. We also note that for high Yb^{3+} concentrations, the inverted ions population increases near $z = 0$, with increased reabsorption losses. This, in turn, increases the initial undershoot in the

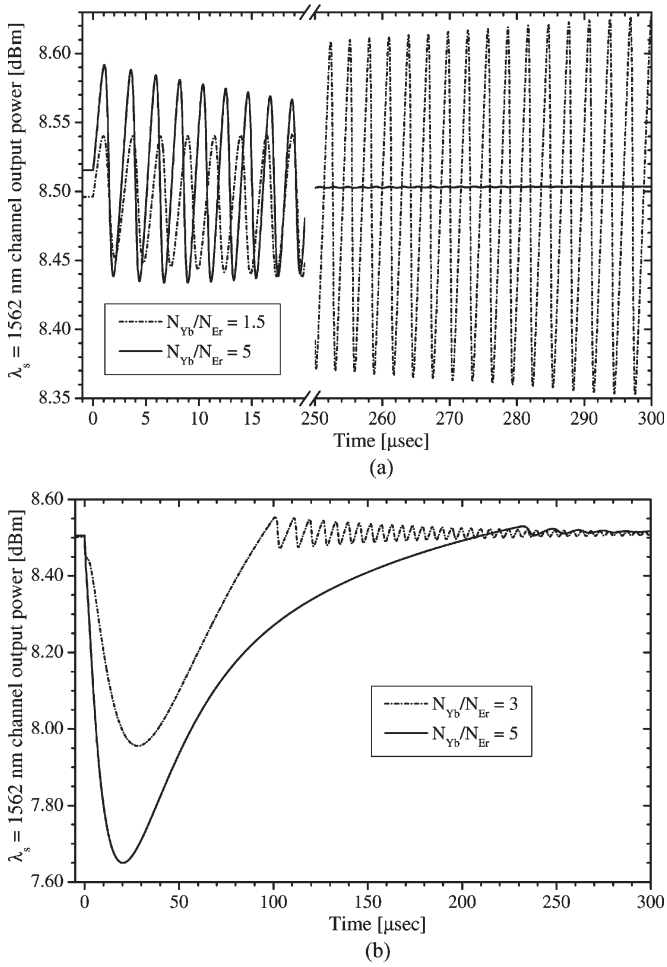

Fig. 4. Transient response of the $\lambda_s = 1562$ nm channel output power, when nine channels are (a) dropped and (b) added at $t = 0$ from initially steady state, for different Yb^{3+}-Er^{3+} ratios. The fiber length is $L = 16.5$ cm, and the relative number of Er^{3+} ions in clusters is $k = 0.17$.

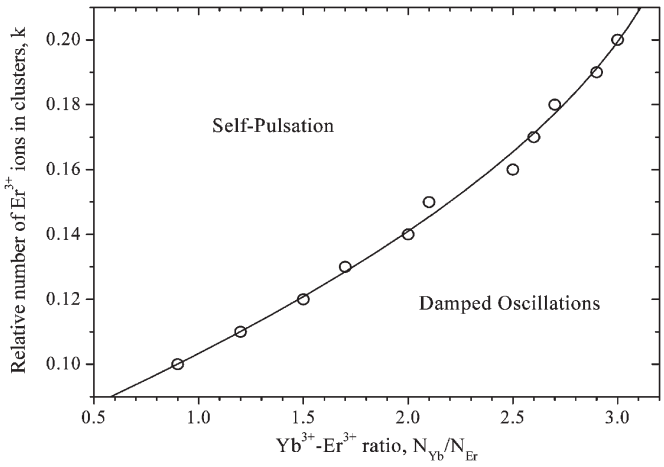

Fig. 5. Calculated stability diagram as function of the Yb^{3+}-Er^{3+} ratio $(N_{\rm Yb}/N_{\rm Er})$ and the relative number of Er^{3+} ions in clusters (k). The circles represent the exact numerical solution, whereas the solid line denotes a parabolic interpolation to the exact solution. The fiber length is $L = 16.5$ cm.

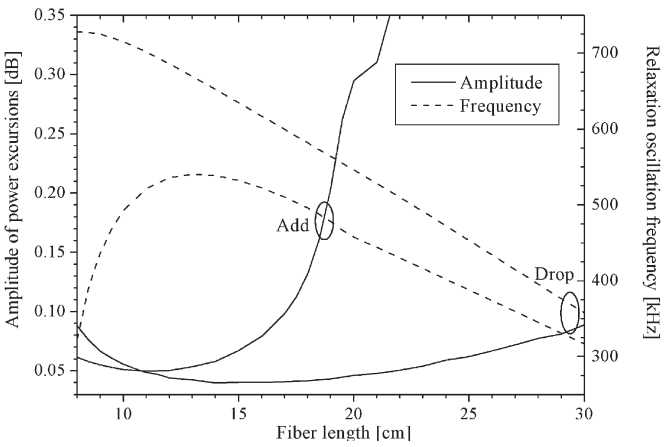

Fig. 6. Dependence of the amplitude of power excursions of the $\lambda_s = 1562$ nm channel (solid line) and the average relaxation oscillation frequency (dashed line) on the fiber length L.

surviving signal output power in the add case [cf. Fig. 4(b)] and delays the onset of relaxation oscillation.

Fig. 5 depicts the parameter $k_{\rm cr}$ (the limiting value for the onset of instability) as function of the Yb^{3+}-Er^{3+} ratio. We note that $k_{\rm cr}$ increases monotonically with the Yb^{3+}-Er^{3+} ratio because stronger effective pumping power is required to bleach the upconversion process in Er^{3+} clusters and to converge to a constant steady state (cf. Fig. 2). We conclude that the presence of Yb^{3+} ions tends to stabilize the surviving signal output in high-concentration gain-clamped EYDFAs, even with a large number of Er^{3+} clusters. These results are in qualitative agreement with perturbation analysis of the Er^{3+}-Yb^{3+} codoped system [12].

Fig. 6 summarizes the dependence of the amplitude of the power excursions (defined as the absolute sum of the maximum overshoot and undershoot of the surviving signal power [18]) and the relaxation oscillation frequency (average of the initial 100 periods) on the fiber length. There exists a fiber length for which this amplitude is the smallest one. This particular length is different for the drop and add cases. For shorter or longer fiber lengths, the compensating laser power becomes smaller, and the laser oscillations deplete the inverted population of Er^{3+} ions more efficiently upon channel removal, which, in turn, increases the amplitude of power excursions. We note that the dynamic response of a fiber with lengths from $L \simeq 8$ cm (lower limit for laser threshold) to $L \simeq 17.5$ cm is acceptable, as the amplitude of power excursions is less than a fraction of decibel in both the add and drop cases [15]. In particular, the dynamic response of a fiber with a flattest gain $(L \simeq 16.5$ cm$)$ allows acceptable compromise between flatness and dynamic performance when designing high-concentration gain-clamped EYDFAs. The relatively small amplitude of the power excursions demonstrated in Fig. 6 is a consequence of the high Er^{3+} concentration assumed in our calculations. If one assumes a lower Er^{3+} concentration, e.g., $N_{\rm Er} = 4 \times 10^{26}$ m^{-3}, one obtains different minimum power excursions amplitude ~ 0.12 dB, with fiber length of $L \simeq 19$ cm, in the drop case. We also note that the increase in the power excursions in longer fiber lengths is more significant in the add case than in the drop case. In particular, for fibers longer than $L \simeq 20$ cm, reabsorption losses become significant, and stable gain-clamping conditions cannot be obtained without additional increase in the pump power. For such long fibers, the delay in the onset of relaxation

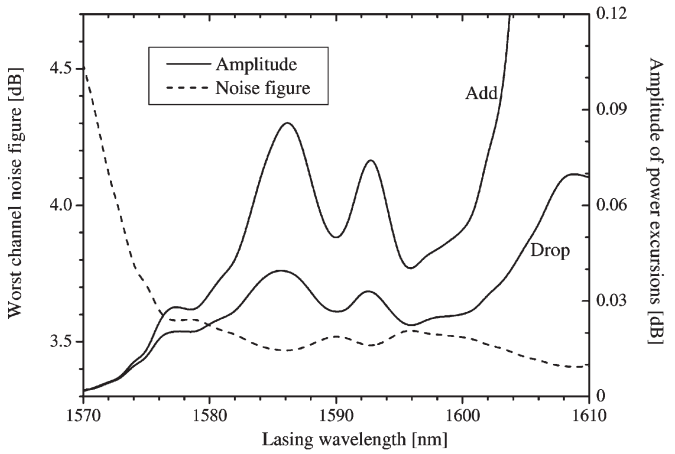

Fig. 7. Dependence of the amplitude of power excursions of the $\lambda_s = 1562$ nm channel (solid line) and the worst channel noise figure (dashed line) of gain-flattened EYDFA on the lasing wavelength. The solid line represents a B-spline interpolation to the exact numerical solution.

oscillation is much bigger than the oscillations period ($\Delta t_{\rm oc} > 3T_{\rm oc}$), so that the contribution of the initial signal undershoot to the amplitude of power excursions becomes dominant. The dependence of the relaxation oscillation frequency on the fiber length is an interplay between the average gain, propagation time, lasing power, and saturation power [18]. In particular, on increasing the fiber length, the average inversion along the fiber (and hence the average gain) decreases, whereas the round-trip time of propagation in the cavity increases. Thus, the average relaxation oscillation frequency of the surviving channel decreases on sufficiently increasing the fiber length [18]. Furthermore, it is higher in the drop case than in the add case, in agreement with the results for low-concentration gain-clamped EDFAs [15], [17].

In the next examples we consider EYDFA with optimal length, i.e., for which the gain flatness is maximized [21]. Fig. 7 shows the effect of the feedback laser wavelength on both the ASE-induced worst channel noise figure [36] and the amplitude of the power excursions. The noise figure dependence on the laser wavelength is a consequence of both the signal gain and the amount of ASE propagating in the signal band. In particular, the ASE power depends on the spatial variation of the population inversion along the fiber length [36]. The noise figure is higher at shorter laser wavelengths, where the power of the compensating laser is stronger, and is nearly constant for longer wavelengths, i.e., for $\lambda > 1575$ nm. On the other hand, the amplitude of the power excursions depends mainly on the spectral properties of the gain and generally increases at the longer laser wavelengths. In particular, on increasing the lasing wavelength, the lasing process becomes less efficient due to the decrease in the Er^{3+} emission cross section. Also, reabsorption due to excess of Er^{3+} clusters becomes weaker, which increases $k_{\rm cr}$ and stabilizes gain-clamping conditions. We conclude that choosing a laser wavelength in the spectral range from $\lambda \simeq 1594$ nm to $\lambda \simeq 1600$ nm allows minimum amplitude of power excursions in both the add and drop cases, with acceptable noise figure performance.

The effect of the Yb^{3+} concentration on the dynamics of gain-clamped EYDFA is further illustrated in Fig. 8. Here, we

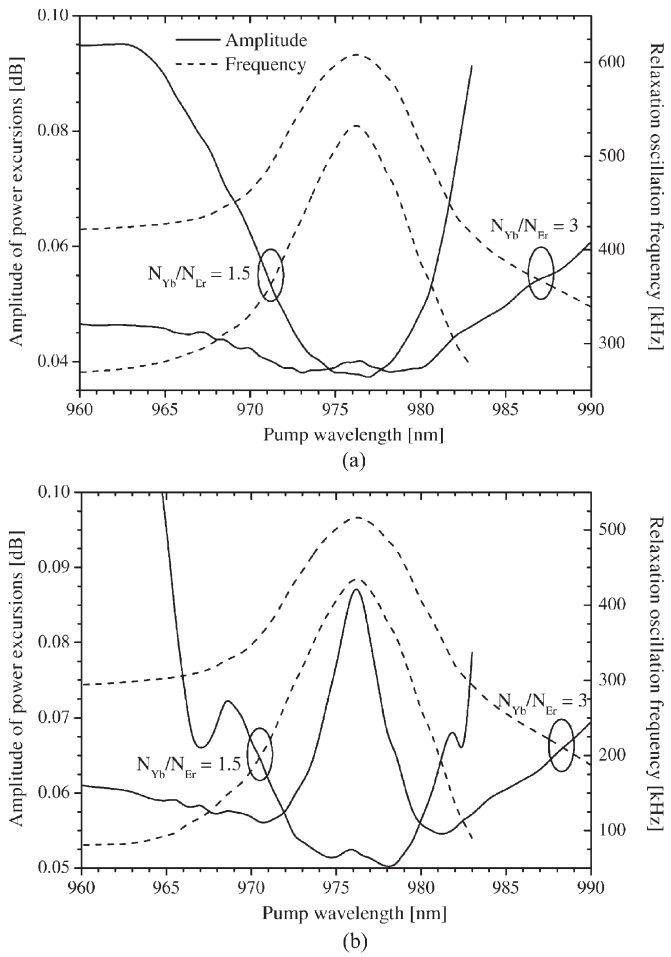

Fig. 8. Dependence of the amplitude of power excursions of the $\lambda_s = 1562$ nm channel (solid line) and the average relaxation oscillation frequency (dashed line) of gain-flattened EYDFA on the pump wavelength λ_p. Two different Yb^{3+}-Er^{3+} ratios are shown in (a) drop and (b) add cases. The solid line represents a B-spline interpolation to the exact numerical solution.

show the dependence of the dynamic parameters on the pump wavelength for two values of Yb^{3+} concentrations. In the drop case, the amplitude of power excursions is generally smaller near the peak Er^{3+} and Yb^{3+} absorption band, i.e., around $\lambda_p = 976$ nm [Fig. 8(a)]. On the other hand, in the add case, the amplitude generally increases at $\lambda_p = 976$ nm in the limit of large Yb^{3+}-Er^{3+} ratio [Fig. 8(b)]. The amplitude increase is substantial at shorter pump wavelengths in the limit of smaller Yb^{3+}-Er^{3+} ratios. In this case, less efficient pump absorption along the fiber, and hence, larger reabsorption losses result in increased contribution of the initial signal power undershoot to the excursions amplitude. Furthermore, under these conditions, $k_{\rm cr}$ is smaller, and gain-clamping becomes unstable in the presence of excess Er^{3+} clustering. We also note that for both the add and drop cases, the relaxation oscillation frequency has a maximum close to $\lambda_p \simeq 976$ nm and that the frequency of oscillations increases on employing higher Yb^{3+}-Er^{3+} ratio. Thus, short fibers with high Yb^{3+} concentration allow more stable gain-clamping conditions over a somewhat broader pumping bandwidth, with reduced sensitivity of the power excursion to variations in the pump wavelength compared with gain-clamped EDFAs. It is worth mentioning, however, that in

the gain-clamping regime, the choice of the pump wavelength almost does not affect the Er^{3+} inversion and, hence, the cavity design, i.e., the optimal flattest gain fiber length [21].

Finally, we consider the effect of the pump power and cavity losses on the gain-clamped EYDFA dynamics. These important design parameters allow extending the dynamic range of input signal powers for which particular gain-clamping conditions can be achieved. On decreasing the output mirror reflectivity at the laser wavelength from $R_2 = 0.04$ to $R_2 = 0.02$, the signal amplification becomes more efficient, and the average gain increases from $\sim$ 19 to $\sim$ 23 dB, respectively. However, increasing the losses also increases the length of a gain-flattened fiber to $\sim$ 20 cm, and the threshold pump power for achieving gain-clamping conditions increases from $P_p^+(0) \simeq 0.7$ W to $P_p^+(0) \simeq 1.8$ W, respectively. For weak pumping just above the threshold, the power excursions are more severe, in particular, for mirror reflectivity $R_2 = 0.02$, where the amplitude of power excursions can be as high as $\sim$ 0.18 dB. On increasing the pump power, the amplitude of power excursions decreases, and the relaxation oscillation frequency increases. In conclusion, we note that the effect of increasing the pump power is similar to increasing the Yb^{3+} concentration, i.e., it increases $k_{\rm cr}$ and, hence, suppresses self-pulsation in the presence of excess Er^{3+} clustering. However, because pumping of Er^{3+} is mainly indirect, the effect of pumping in suppressing self-pulsation depends heavily on the Yb^{3+}-Er^{3+} energy-transfer efficiency. Furthermore, increasing the pump power reduces the signal conversion efficiency because the gain is fixed.

IV. Conclusion

Time-dependent rate-propagation equations were used to study the dynamic features of high-concentration gain-clamped short EYDFAs, operating in the gain-flattened regime. Our results suggest that centimeters-long EYDFAs are attractive candidates for reconfigurable WDM networks, provided that the number of Er^{3+} ions in clusters is kept small. In particular, we demonstrated that the amplitude of power excursions in the surviving channel is typically small, e.g., less than 0.1 dB, for a wide range of practical operating conditions. These power excursions are much smaller than the corresponding figures in conventional gain-clamped EDFAs [15]–[18] and relatively long gain-clamped EYDFAs [19], [20]. Also, polarization effects are expected to be considerably smaller in circular, short EYDFAs compared with the recently proposed high-concentration Er^{3+}-doped waveguide amplifiers for similar WDM applications [37]. We suggest that further engineering of the glass host properties may extend the gain bandwidth of short EYDFAs.

We have shown that the noise penalty due to gain-clamping becomes smaller on selecting a feedback laser channel with wavelength sufficiently longer than the WDM signal bandwidth, i.e., $\lambda > 1575$ nm. On the other hand, increasing the laser wavelength also increases the amplitude of the dynamic power excursions, in particular in the add case.

The dynamic characteristics of the relaxation oscillations in the surviving signal are strongly dependent on the effective pumping rate of the Er^{3+} ions and on the degree of Er^{3+} clustering. In particular, a high number of Er^{3+} ions in clusters result in unstable gain-clamping conditions. This instability is characterized by undamped oscillations of the surviving signal in the drop case and deep signal power undershoot in the add case. Increasing the Yb^{3+}-Er^{3+} ratio allows achieving stable gain-clamping conditions over a broader bandwidth of pump wavelengths, with lower sensitivity of the dynamic power excursions to fluctuations in the pump wavelength. Furthermore, employing higher Yb^{3+} concentrations increases the pump absorption and reduces the period of relaxation oscillations. This, in turn, effectively suppresses clustering-induced nondamping oscillations in the laser channel, provided that the Yb^{3+} concentration is higher than a certain limiting value that depends on the degree of Er^{3+} clustering. On the other hand, reabsorption losses become more significant, increasing the initial signal output power undershoot in the add case. Thus, the optimum fiber length is a compromise between acceptable dynamic performance and the efficiency of the pump absorption.

Appendix
Finite-Difference Approximations

The rate of change of the spectral power densities per unit wavelength $P_{\rm Er}^{\pm}(z,t,\lambda)$ that are emitted and amplified due to Er^{3+} transitions is given by [21]

$$\pm\frac{dP_{\rm Er}^{\pm}(z,t,\lambda)}{dz} = \big(\Gamma(\lambda)\left\{\left[N_2(z,t)+\bar{N}_2(z,t)\right]\sigma_{21}(\lambda) - \sigma_{12}(\lambda)\left[N_1(z,t)+\bar{N}_1(z,t)\right]\right\}-\alpha\big) \times P_{\rm Er}^{\pm}(z,t,\lambda)+\Gamma(\lambda)P_0(\lambda)\sigma_{21}(\lambda) \times \left[N_2(z,t)+\bar{N}_2(z,t)\right] \quad \text{(A1)}$$

where $dP_{\rm Er}^{\pm}(z,t,\lambda)/dz \equiv \partial P_{\rm Er}^{\pm}/\partial z \pm (n/c)\partial P_{\rm Er}^{\pm}/\partial t$, and n is the refractive index of the core. Here, the terms N_2 ($\bar{N}_2$) and N_1 ($\bar{N}_1$) correspond to the excited and ground state populations of homogeneous (clustered) Er^{3+} ions, respectively. The spectral power density term $P_0(\lambda)$ in (A1) represents the contribution of the spontaneous emission to the two orthogonal polarizations of the guided mode [21]. To solve (A1), we assume equally spaced intervals along the z-axis with spatial points $z_j = j\Delta z$ ($j = 1,2,\ldots,j_{\max}$) and time points $t_i = i\Delta t$ ($i = 1,2,\ldots,i_{\max}$). We use two different grids to discritize the photons and ions equations [21], which are half-step $\Delta t/2$ and half-step $\Delta z/2$ staggered in time and space, respectively. Thus, the spectral power densities $(P_{\rm Er}^{\pm})_{i,j}$ are defined at point (i,j) of the photons grid and at wavelength λ. We obtain finite-difference approximations, e.g., as follows:

$$\left(P_{\rm Er}^{+}\right)_{i,j} = \left\{\left(P_{\rm Er}^{+}\right)_{i-1,j-1}\left[G_{i,j}+\frac{n}{2c}\frac{1}{\Delta t}\right] + \left(P_{\rm Er}^{+}\right)_{i-1,j}\left[\frac{n}{2c}\frac{1}{\Delta t}\right] + \left(P_{\rm Er}^{+}\right)_{i,j-1}\left[\frac{1}{\Delta z}-\frac{n}{2c}\frac{1}{\Delta t}\right]+F_{i,j}\right\} \cdot\left\{\frac{1}{\Delta z}+\frac{n}{2c}\frac{1}{\Delta t}-G_{i,j}\right\}^{-1} \quad \text{(A2)}$$

$$\left(P_{\mathrm{Er}}^{-}\right)_{i,j-1}=\left\{\left(P_{\mathrm{Er}}^{-}\right)_{i-1,j}\left[G_{i,j}+\frac{n}{2c}\frac{1}{\Delta t}\right]+\left(P_{\mathrm{Er}}^{-}\right)_{i-1,j-1}\left[\frac{n}{2c}\frac{1}{\Delta t}\right]+\left(P_{\mathrm{Er}}^{-}\right)_{i,j}\left[\frac{1}{\Delta z}-\frac{n}{2c}\frac{1}{\Delta t}\right]+F_{i,j}\right\}\cdot\left\{\frac{1}{\Delta z}+\frac{n}{2c}\frac{1}{\Delta t}-G_{i,j}\right\}^{-1} \tag{A3}$$

where $F_{i,j}$ and $G_{i,j}$ are quantities defined on point (i,j) of the ions grid and are given by

$$F_{i,j}\equiv\Gamma(\lambda)P_0(\lambda)\sigma_{21}(\lambda)\left[(N_2)_{i,j}+(\bar{N}_2)_{i,j}\right] \tag{A4}$$

$$G_{i,j}\equiv\frac{1}{2}\left[\Gamma(\lambda)\left\{\left[(N_2)_{i,j}+(\bar{N}_2)_{i,j}\right]\sigma_{21}(\lambda)-\sigma_{12}(\lambda)\left[(N_1)_{i,j}+(\bar{N}_1)_{i,j}\right]\right\}-\alpha\right]. \tag{A5}$$

Note that for the polarized signal channels, we multiply the RHS of (A4) by a factor of 1/2. Similarly, it is straightforward to obtain finite-difference approximations for the Yb^{3+} spectral power densities and the pump power, which have the same form as (A2) and (A3), but with modifications to (A4) and (A5).

To solve the finite-difference equations, we assume that the terms $F_{i,j}$ and $G_{i,j}$ are all known for the row i of the ions grid. Furthermore, we assume that $(P_{\mathrm{Er}}^{\pm})_{i-1,j}$ are known for all values of j and that $(P_{\mathrm{Er}}^{+})_{i,j-1}$ [or $(P_{\mathrm{Er}}^{-})_{i,j}$] is also known. Under these assumptions, the numerical solution of (A2) and (A3) on row i of the photons grid starts from the boundary $j=1(z=0)$ or $j=j_{\max}$ $(z=L)$. However, in case that both $R_1(\lambda)\neq 0$ and $R_2(\lambda)\neq 0$, e.g., in lasers, the boundary condition (1) is given in an implicit form. That is, e.g., at $j=1$, we have $(P_{\mathrm{Er}}^{+})_{i,1}$ given in terms of the unknown quantity $(P_{\mathrm{Er}}^{-})_{i,1}$. To express the boundary conditions exactly in an explicit form, we employ (A2) in a recursive manner for $(P_{\mathrm{Er}}^{+})_{i,j-1}, (P_{\mathrm{Er}}^{+})_{i,j-2},\ldots,(P_{\mathrm{Er}}^{+})_{i,2}$ to obtain

$$\left(P_{\mathrm{Er}}^{+}\right)_{i,j}=U_{i,j}^{+}\left(P_{\mathrm{Er}}^{+}\right)_{i,1}+V_{i,j}^{+} \tag{A6}$$

where $U_{i,j}^{+}$ and $V_{i,j}^{+}$ are constants independent of $(P_{\mathrm{Er}}^{+})_{i,1}$. Thus, in (A6), the term $(P_{\mathrm{Er}}^{+})_{i,j}$ is expressed as a linear function of an initial guess $(P_{\mathrm{Er}}^{+})_{i,1}$. A similar expression for $(P_{\mathrm{Er}}^{-})_{i,j-1}$ can be derived from (A3), i.e.,

$$\left(P_{\mathrm{Er}}^{-}\right)_{i,j-1}=U_{i,j-1}^{-}\left(P_{\mathrm{Er}}^{-}\right)_{i,j_{\max}}+V_{i,j-1}^{-} \tag{A7}$$

with constant coefficients $U_{i,j-1}^{-}$ and $V_{i,j-1}^{-}$ that are independent of $(P_{\mathrm{Er}}^{-})_{i,j_{\max}}$. Assigning $j=j_{\max}$ in (A6) and $j=2$ in (A7), and using the boundary conditions (1), i.e., $(P_{\mathrm{Er}}^{-})_{i,j_{\max}}=R_2(\lambda)(P_{\mathrm{Er}}^{+})_{i,j_{\max}}$ and $(P_{\mathrm{Er}}^{+})_{i,1}=R_1(\lambda)(P_{\mathrm{Er}}^{-})_{i,1}$, we obtain

$$\left(\tilde{P}_{\mathrm{Er}}^{+}\right)_{i,1}=Q_1\left(P_{\mathrm{Er}}^{+}\right)_{i,1}+Q_2 \tag{A8}$$

where Q_1 and Q_2 are two constants independent of the initial guess $(P_{\mathrm{Er}}^{+})_{i,1}$, and $(\tilde{P}_{\mathrm{Er}}^{+})_{i,1}$ is the new value obtained for $(P_{\mathrm{Er}}^{+})_{i,1}$ after one round trip in the cavity. The exact value for $(P_{\mathrm{Er}}^{+})_{i,1}$ satisfies $(\tilde{P}_{\mathrm{Er}}^{+})_{i,1}=(P_{\mathrm{Er}}^{+})_{i,1}$, and therefore

$$\left(P_{\mathrm{Er}}^{+}\right)_{i,1}=\frac{Q_2}{1-Q_1}. \tag{A9}$$

To calculate the constants Q_1 and Q_2, we start with an initial guess for $(P_{\mathrm{Er}}^{+})_{i,1}$, namely, $(P_{\mathrm{Er}}^{+})_{i,1}^{(1)}$, and solve (A2) and (A3) to obtain $(P_{\mathrm{Er}}^{+})_{i,1}^{(2)}$ after one round trip and $(P_{\mathrm{Er}}^{+})_{i,1}^{(3)}$ after the next round trip. The calculated values must satisfy (A8), so that the unknowns Q_1 and Q_2 can be solved, and the exact $(P_{\mathrm{Er}}^{+})_{i,1}$ is obtained from (A9). In particular, for $(P_{\mathrm{Er}}^{+})_{i,1}^{(1)}=0$, we find that

$$\left(P_{\mathrm{Er}}^{+}\right)_{i,1}\equiv\frac{\left[\left(P_{\mathrm{Er}}^{+}\right)_{i,1}^{(2)}\right]^2}{2\left(P_{\mathrm{Er}}^{+}\right)_{i,1}^{(2)}-\left(P_{\mathrm{Er}}^{+}\right)_{i,1}^{(3)}}. \tag{A10}$$

The exact $(P_{\mathrm{Er}}^{+})_{i,1}$ and the calculated $(P_{\mathrm{Er}}^{+})_{i,j}^{(1)}$ and $(P_{\mathrm{Er}}^{+})_{i,j}^{(2)}$ from the two round trips are used to find the exact $(P_{\mathrm{Er}}^{+})_{i,j}$ along the fiber for all $j\neq 1$. To this end, we note that both $(P_{\mathrm{Er}}^{+})_{i,j}^{(1)}$ and $(P_{\mathrm{Er}}^{+})_{i,j}^{(2)}$ satisfy (A6), so that the constants $U_{i,j}^{+}$ and $V_{i,j}^{+}$ are known in principle. Again, for $(P_{\mathrm{Er}}^{+})_{i,1}^{(1)}=0$, we find that for all $j\neq 1$

$$\left(P_{\mathrm{Er}}^{+}\right)_{i,j}=\left[\frac{\left(P_{\mathrm{Er}}^{+}\right)_{i,j}^{(2)}-\left(P_{\mathrm{Er}}^{+}\right)_{i,j}^{(1)}}{\left(P_{\mathrm{Er}}^{+}\right)_{i,1}^{(2)}}\right]\left(P_{\mathrm{Er}}^{+}\right)_{i,1}+\left(P_{\mathrm{Er}}^{+}\right)_{i,j}^{(1)}. \tag{A11}$$

Similarly, because also $(P_{\mathrm{Er}}^{-})_{i,j-1}$ depends linearly on $(P_{\mathrm{Er}}^{+})_{i,1}$, we find that for all $j\neq 1$

$$\left(P_{\mathrm{Er}}^{-}\right)_{i,j-1}=\left[\frac{\left(P_{\mathrm{Er}}^{-}\right)_{i,j-1}^{(2)}-\left(P_{\mathrm{Er}}^{-}\right)_{i,j-1}^{(1)}}{\left(P_{\mathrm{Er}}^{+}\right)_{i,1}^{(2)}}\right]\left(P_{\mathrm{Er}}^{+}\right)_{i,1}+\left(P_{\mathrm{Er}}^{-}\right)_{i,j-1}^{(1)}. \tag{A12}$$

Thus, using (A11) and (A12), we calculate the exact values $(P_{\mathrm{Er}}^{+})_{i,j}$ and $(P_{\mathrm{Er}}^{-})_{i,j-1}$ with the exact boundary conditions. We note that if $R_1(\lambda)=0$ and/or $R_2(\lambda)=0$, the whole procedure is not necessary because the power at row i is exactly known, at least, on one of the two boundaries.

REFERENCES

[1] M. R. X. de Barros, G. Nykolak, D. J. DiGiovanni, A. Bruce, W. H. Grodkiewicz, and P. C. Becker, "Performance of a high concentration Er^{3+}-doped alumino silicate fiber amplifier," *IEEE Photon. Technol. Lett.*, vol. 8, no. 6, pp. 761–763, Jun. 1996.

[2] B. C. Hwang, S. Jiang, T. Luo, J. Watson, G. Sorbello, and N. Peyghambarian, "Cooperative upconversion and energy transfer of new high Er^{3+}- and Er^{3+}-Yb^{3+}-doped phosphate glasses," *J. Opt. Soc. Amer. B, Opt. Phys.*, vol. 17, no. 5, pp. 833–839, May 2000.

[3] B. C. Hwang, S. Jiang, T. Luo, K. Seneschal, G. Sorbello, M. Morrell, F. Smektala, S. Honkanen, J. Lucas, and N. Peyghambarian, "Performance of high-concentration Er^{3+}-doped phosphate fiber amplifiers," *IEEE Photon. Technol. Lett.*, vol. 13, no. 3, pp. 197–199, Mar. 2001.

[4] Y. Hu, S. Jiang, T. Luo, K. Seneschal, M. Morrell, F. Smektala, S. Honkanen, J. Lucas, and N. Peyghambarian, "Performance of

high-concentration Er^{3+}-Yb^{3+}-codoped phosphate fiber amplifiers," *IEEE Photon. Technol. Lett.*, vol. 13, no. 7, pp. 657–659, Jul. 2001.
[5] M. I. Hayee and A. E. Willner, "Transmission penalties due to EDFA gain transients in add-drop multiplexed WDM networks," *IEEE Photon. Technol. Lett.*, vol. 11, no. 7, pp. 889–891, Jul. 1999.
[6] M. Zirngibl, "Gain control in erbium-doped fibre amplifiers by an all-optical feedback loop," *Electron. Lett.*, vol. 27, no. 7, pp. 560–561, Mar. 1991.
[7] E. Delevaque, T. Georges, J. F. Bayon, M. Monerie, P. Niay, and P. Bernage, "Gain control in erbium-doped fibre amplifiers by lasing at 1480 nm with photoinduced Bragg gratings written on fibre ends," *Electron. Lett.*, vol. 29, no. 12, pp. 1112–1114, Jun. 1993.
[8] C. Jiang, W. Hu, and Q. Zeng, "Improved gain characteristics of high concentration erbium-doped phosphate fiber amplifier," *IEEE Photon. Technol. Lett.*, vol. 16, no. 3, pp. 774–776, Mar. 2004.
[9] ——, "Numerical analysis of concentration quenching model of Er^{3+}-doped phosphate fiber amplifier," *IEEE J. Quantum Electron.*, vol. 39, no. 10, pp. 1266–1271, Oct. 2003.
[10] F. Sanchez, P. L. Boudec, P. L. Francois, and G. Stephan, "Effects of ion pairs on the dynamics of erbium-doped fiber lasers," *Phys. Rev. A, Gen. Phys.*, vol. 48, no. 3, pp. 2220–2229, Sep. 1993.
[11] H. L. An, E. Y. B. Pun, H. D. Liu, and X. Z. Lin, "Effects of ion clusters on the performance of a heavily doped erbium-doped fiber laser," *Opt. Lett.*, vol. 23, no. 15, pp. 1197–1199, Aug. 1998.
[12] M. Ding and P. K. Cheo, "Effects of Yb:Er-codoping on suppressing self-pulsing in Er-doped fiber lasers," *IEEE Photon. Technol. Lett.*, vol. 9, no. 3, pp. 324–326, Mar. 1997.
[13] X. L. Huang, H. Y. Chen, Y. Z. Liu, J. Z. Dai, Y. P. Yang, and J. Q. Song, "Study on double-cladding erbium–ytterbium codoped phosphate glass fiber amplifiers," in *Proc. Conf. Commun. Circuits Syst. West Sino Expo.*, Chengdu, China, 2002, vol. 1, pp. 816–818.
[14] Y. J. Deiss, C. M. McIntosh, G. M. Williams, and J. M. P. Delavaux, "Gain flatness of a 30 dBm tandem Er^{3+}-Er^{3+}/Yb^{3+} double-clad fiber amplifier for WDM transmission," in *Proc. Opt. Fiber Commun. Conf.*, Anaheim, CA, 2002, vol. 70, pp. 249–251.
[15] G. Luo, J. L. Zyskind, J. A. Nagel, and M. A. Ali, "Experimental and theoretical analysis of relaxation-oscillations and spectral hole burning effects in all-optical gain-clamped EDFA's for WDM networks," *J. Lightw. Technol.*, vol. 16, no. 4, pp. 527–533, Apr. 1998.
[16] D. H. Richards, J. L. Jackel, and M. A. Ali, "A theoretical investigation of dynamic all-optical automatic gain control in multichannel EDFA's and EDFA cascades," *IEEE J. Sel. Topics Quantum Electron.*, vol. 3, no. 4, pp. 1027–1036, Aug. 1997.
[17] A. Bononi and L. Barbieri, "Design of gain-clamped doped-fiber amplifiers for optimal dynamic performance," *J. Lightw. Technol.*, vol. 17, no. 7, pp. 1229–1240, Jul. 1999.
[18] Q. Yu and C. Fan, "Simple dynamic model of all-optical gain-clamped erbium-doped fiber amplifiers," *J. Lightw. Technol.*, vol. 17, no. 7, pp. 1166–1171, Jul. 1999.
[19] K. Ennser, G. Sacchi, C. Mornatta, and S. Taccheo, "Dynamic behavior of gain-clamped Er:Yb and high concentration Er-doped amplifier," *IEEE Photon. Technol. Lett.*, vol. 16, no. 7, pp. 1643–1645, Jul. 2004.
[20] ——, "Modeling and investigation of transient response in gain clamped Er–Yb and high concentration Er doped amplifier," in *Proc. Conf. Opt. Fiber Commun. Postconf. Dig.*, Washington, DC, 2004, pp. 172–174.
[21] E. Yahel and A. Hardy, "Efficiency optimization of high-power, Er^{3+}-Yb^{3+}-codoped fiber amplifiers for wavelength-division-multiplexing applications," *J. Opt. Soc. Amer. B, Opt. Phys.*, vol. 20, no. 6, pp. 1189–1197, Jun. 2003.
[22] A. W. Snyder and J. D. Love, *Optical Waveguide Theory*. New York: Chapman & Hall, 1983.
[23] A. Liu and K. Ueda, "The absorption characteristics of circular, offset, and rectangular double-clad fibers," *Opt. Commun.*, vol. 132, no. 5/6, pp. 511-518, Dec. 1996.
[24] M. J. F. Digonnet, M. K. Davis, and R. H. Pantell, "Rate equations for clusters in rare earth-doped fibers," *Opt. Fiber Technol.*, vol. 1, no. 1, pp. 48–58, Oct. 1994.
[25] C. Jiang, W. Hu, and Q. Zeng, "Improved gain performance of high concentration Er^{3+}-Yb^{3+}-codoped phosphate fiber amplifier," *IEEE J. Quantum Electron.*, vol. 41, no. 5, pp. 704–708, May 2005.
[26] P. F. Wysocki, "Erbium-doped fiber amplifiers: Advanced topics," in *Rare-Earth-Doped Fiber Lasers and Amplifiers*, 2nd ed. M. J. F. Digonnet, Ed. New York: Marcel Dekker, 2001, pp. 583–680.
[27] G. A. Sefler, W. D. Mack, G. C. Valley, and T. S. Rose, "Secondary energy transfer and nonparticipatory Yb^{3+} ions in Er^{3+}-Yb^{3+} high-power amplifier fibers," *J. Opt. Soc. Amer. B, Opt. Phys.*, vol. 21, no. 10, pp. 1740–1748, Oct. 2004.
[28] M. Federighi and F. Di Pasquale, "The effect of pair-induced energy transfer on the performance of silica waveguide amplifiers with high Er^{3+}/Yb^{3+} concentrations," *IEEE J. Quantum Electron.*, vol. 7, no. 3, pp. 303–305, Mar. 1995.
[29] I. Kelson and A. A. Hardy, "Strongly pumped fiber lasers," *IEEE J. Quantum Electron.*, vol. 34, no. 9, pp. 1570–1577, Sep. 1998.
[30] M. Achtenhagen, R. J. Beeson, F. Pan, B. Nyman, and A. Hardy, "Gain and noise in ytterbium sensitized erbium doped amplifiers: Measurement and simulations," *J. Lightw. Technol.*, vol. 19, no. 10, pp. 1521–1526, Oct. 2001.
[31] Y. Huo, P. K. Cheo, and G. G. King, "Modeling and experiments of actively Q-switched Er^{3+}-Yb^{3+} codoped clad-pumped fiber lasers," *IEEE J. Quantum Electron.*, vol. 41, no. 4, pp. 573–580, Apr. 2005.
[32] S. Jiang, T. Luo, B. C. Hwang, G. Nunzi-Conti, M. Myers, D. Rhonehouse, S. Honkanen, and N. Peyghambarian, "New Er^{3+}-doped phosphate glass for ion-exchanged waveguide amplifiers," *Opt. Eng.*, vol. 37, no. 12, pp. 3282–3286, Dec. 1998.
[33] S. Taccheo, G. Sorbello, S. Longhi, and P. Laporta, "Measurement of the energy transfer and upconversion constants in Er–Yb-doped phosphate glass," *Opt. Quantum Electron.*, vol. 31, no. 3, pp. 249–262, Mar. 1999.
[34] G. C. Valley, "Modeling cladding-pumped Er/Yb fiber amplifiers," *Opt. Fiber Technol.*, vol. 7, no. 1, pp. 21–44, Jan. 2001.
[35] M. K. Davis, M. J. F. Digonnet, and R. H. Pantell, "Characterization of clusters in rare earth-doped fibers by transmission measurements," *J. Lightw. Technol.*, vol. 13, no. 2, pp. 120–126, Feb. 1995.
[36] E. Yahel and A. Hardy, "Amplified spontaneous emission in high-power, Er^{3+}-Yb^{3+}-codoped fiber amplifiers for wavelength-division-multiplexing applications," *J. Opt. Soc. Amer. B, Opt. Phys.*, vol. 20, no. 6, pp. 1198–1203, Jun. 2003.
[37] K. Ennser, G. Della Valle, M. Ibsen, J. Shmulovich, and S. Taccheo, "Erbium-doped waveguide amplifier for reconfigurable WDM metro networks," *IEEE Photon. Technol. Lett.*, vol. 17, no. 7, pp. 1468–1470, Jul. 2005.

Eldad Yahel received the B.Sc. degree in physics and materials engineering from Ben-Gurion University of the Negev, Beer-Sheva, Israel, in 1998 and the M.Sc. degree in electrical engineering from Tel Aviv University, Tel Aviv, Israel, in 2002. He is currently working toward the Ph.D. degree at the Advanced Technology Institute, University of Surrey, Guildford, U.K.

From 1999 to 2002, he was with the Department of Electrical Engineering-Physical Electronics, Tel Aviv University, Israel, conducting research on Er^{3+}-Yb^{3+} codoped fiber lasers and amplifiers.

Ortwin Hess received the B.Sc. degree in physics from the University of Erlangen, Nuremberg, Germany, in 1987 and the M.Sc. and Ph.D. degrees from the Technical University of Berlin, Berlin, Germany, in 1990 and 1993, respectively. He holds a Habilitation degree in theoretical physics from the University of Stuttgart, Stuttgart, Germany, which he received in 1997.

He is a Professor of computational quantum electronics and leads the Theory and Advanced Computation Group at the Advanced Technology Institute, University of Surrey, Guildford, U.K. He has been a Visiting Professor at Stanford University, Stanford, CA, and the University of Munich, Munich, Germany. His research interests are focused on the supercomputer simulation of the ultrafast spatiotemporal dynamics of semiconductor lasers and novel high-speed optoelectronic devices (quantum dot and quantum well lasers, high-power semiconductor optical amplifiers, and microcavities). His current interests encompass ultrafast effects in active semiconductor media, mesoscopic quantum electronics (quantum fluctuations, microcavity lasers, control of spontaneous emission, optical molecular motors, and biophotonics), photonic materials (quantum dots, photonic crystals, synthetic opals, liquid crystals, and biomolecules), as well as nanothermodynamics and nonlinear nanorheology.

Amos A. Hardy (SM'84–F'97). For photograph and biography, please see this issue, p. 2232.